

Supplemental information

Rapid and continuous magnetic separation in droplet microfluidic devices

Eric Brouzes, Travis Kruse, Robert Kimmerling, Helmut H. Strey

Biomedical Engineering Department
Stony Brook University
Stony Brook, NY 11794-5281

Material and methods

Chip fabrication. Chips are hybrid PDMS/glass chips fabricated using soft-lithography as previously described¹. In brief, microfluidic circuits are designed using the DraftSight software (Dassault Systems, Paris) and printed at 25,400 dpi resolution onto a Fuji transparency mask (CAD/Art Services Inc., Bandon, Or). Using the mask, we make a master with the negative photoresist SU8 (Microchem, MA) onto a 3 inch silicon wafer by photolithography (Newport 500W UV-illumination system). We use PDMS (Sylgard 184, Corning) at 1:10 weight ratio of curing agent: polymer base for molding. After degassing and curing at 80°C for 2 hours, the PDMS slab is punched (Syneo, US), cleaned with tape (Scotch 810 Magic Tape) and finally bonded to a glass slide using an oxygen plasma cleaner (PDC-32G, Harrick plasma). The assembled chip is sandwiched between aluminum plates held by binder clips. After a 80°C overnight incubation, channels are treated with a fluorinated trichloro silane reagent (heptadecafluoro-1,1,2,2-tetrahydrodecyl)trichlorosilane, Gelest, PA) diluted at 1% wt in FC3280 oil (3M). The solution is injected into channels with a disposable syringe, a hydrophobic 0.2 µm disc filter and a blunt needle, and flushed out with FC 3283 oil after a few minutes of incubation.

To control the distance of the magnet to the channel we inserted a series of calibration marks on the master that are parallel to the channel. To cut the PDMS slab at a certain distance, we place the PDMS slab onto a glass slide channels up under a stereomicroscope. We align a second glass slide that will serve as cutting guide along the desired channel mark. The glass slide also covers the channels to protect from uncontrolled cutting. Once aligned, we press gently on the glass slide so that capillarity maintains the guide firmly on the PDMS at the chosen distance. We then cut the PDMS with a 4" razor blade (Extra-Wide Razor Blade Scraper, American Line) using the guide. The exact distance is measured experimentally using the inverted microscope and calculated with calibration marks placed in the design.

Microfluidic set-up. The microfluidic set-up is based on an inverted microscope (Motic, AE31) equipped with a custom stage to accommodate either 25 mm x 75 mm or 75 mm x 75 mm chips. The microscope is equipped with a Firewire camera (Scout scA640-120fm, Basler), and the illumination is accomplished by a high power LED (Luxeon) that is driven by a MOSFET circuit connected to one of the digital output pins of a multifunction data acquisition card (NI PCIe-7841R, National Instruments). Using this setup, we can control and trigger the camera and synchronize the image acquisition and illumination using an application developed in Labview (National Instruments). The system permits stroboscopic exposure in which an image can be captured over the period of 2 illumination pulses. This feature allows the experimental measurement of droplet velocity.

Fluids are actuated with a custom system based on a set of pressure controllers with a 0-15 psi pressure range (MPV1, Proportion Air) mounted in parallel onto a manifold. They are controlled by a Labview application via a microprocessor-based (Arduino) interface using serial communication. Fluids are loaded into 1 mL or 15 mL tubes equipped with custom designed teflon caps that serve as port to connect 1/32" peek tubing (Idex) whose other end is directly inserted in chip inlets and outlets.

Bead encapsulation. We encapsulate 1µm diameter superparamagnetic beads (Oligo d(T)₂₅ Magnetic Beads, New England Biolabs) that are equivalent to Dynabeads MyOne into 70 µm diameter (185 pL) droplets using a flow focusing nozzle (40 µm wide x 50 µm deep x 370 µm long; oil lines are 30 µm wide). Droplets are stabilized in HFE7500 fluorinated oil using a PEG-Krytox surfactant² at 1% weight concentration. Superparamagnetic beads are washed once with Dulbecco PBS to remove surfactant such as Tween present in

the storage buffer. They are then diluted 4-fold into Dulbecco PBS for an average number of 376 beads per droplet (Supp. Fig.2). Droplets are collected into a vessel made of a 3 inch long and 15 mm diameter Trubore glass tubing (Ace glass inc, NJ) capped by 2 custom designed teflon inserts that serve as ports to connect 1/32" peek tubing (Idex). The glass tubing is treated with the same fluorinated tri-chlorosilane solution used for channels to ensure good emulsion stability. It is critical to avoid the presence of a magnetic field during the encapsulation phase to obtain a homogeneous bead distribution. In the presence of a magnetic field, beads repeatedly accumulate and detach in the inlet such that they are encapsulated in staccato bursts (data not shown). We characterized the distribution of the number of beads per droplet by counting beads semi-manually using the Fiji package (<http://fiji.sc/Fiji>) from a series of images taken during the re-injection of the emulsion at low velocity into a dedicated microfluidic channel (75 μm wide and 15 μm deep).

Encapsulation of magnetic beads in the presence of a magnetic field. We used a hydrodynamic focusing nozzle (30 μm wide x 25 μm deep) upstream of a 50 μm wide, 25 μm deep and 17 mm long channel. The microfluidic circuit is similar to the one used to re-inject droplets except for the design of the nozzle. The magnet (1/4"x1/4"x1/4" N52 magnet, K&J Magnetics) was located at 16 mm from the nozzle. Droplets were generated at different throughputs and velocities. We quantified the number of magnetic beads inside droplets by segmenting the magnetic beads and measuring the projected area occupied of the beads. The data represent the analysis of 60 droplets for each condition. The dispersion is defined as the standard deviation normalized by the average number of magnetic beads in droplets.

Absence of marginalization of the magnetic beads in the absence of magnetic field.

Droplets were re-injected at different velocities in the absence of magnet to verify whether possible patterns of internal flows could result into the marginalization of magnetic beads in the absence of a magnet. The minimum projection and average projection data were compiled from 80 different droplets in each condition. We covered the experimental conditions by varying the droplet velocity from 1.1 mm/s to 15.8 mm/s.

Movie of a magnetic-laden droplet in the absence of magnetic field to study internal flows (Supp. Movie 2).

Droplets were re-injected at 3.9 mm/s and observed using a high-speed camera (X-PRI, AOS Technologies AG) at a rate of 500 frames per second and at 20x magnification. About 22 images of full droplets were captured per field of view. Images were cropped, after segmentation, such that droplets would be centered in a minimal image size. Image background was removed and the contrast adjusted using the ImageJ package. The movie is slowed down 70 fold and played at 7 frames per second.

Study of the internal flow field. We used the 22 frames of Supp. Movie 2 to perform an average projection and get an indication of the steady flow field inside droplets. We use the same frames to perform a Particle Image Velocimetry (PIV) analysis using the JPIV package (www.jpiv.vennemann-online.de) with the parameters captured in Supp. Fig. 5. The conditions of image acquisition here are not optimal to perform a PIV analysis because we did not isolate magnetic beads by plane in the z direction, and magnetic beads in other planes (out of focus) can interfere with the analysis; however, the high density of beads used in the experiments tends to conceal the beads present in other planes. Nevertheless, we consider those data as indicative and not quantitative.

Reinjection of magnetic bead containing emulsions. Emulsions were re-injected into a 50 μm wide, 25 μm deep and 17 mm long channel terminated by a splitting fork. The inlet includes an extra port to facilitate the chip priming and operation by allowing the rapid removal of air bubbles or other contaminants. The emulsion is diluted using a flow focusing nozzle and surfactant (1% weight) containing HFE7500 oil. For each experiment, the magnet position and distance to the channel are documented by pictures at low magnification, and determined with the help of marks included along the channel in the design (major marks every mm, minor marks every 100 μm). For each data point, we set and stabilized droplet velocity that was measured both at the beginning and at the end of data collection using our stroboscopic illumination system. Velocities were calculated from a series of images by dividing the measured distances between droplet fronts over the delay

between illumination pulses. Once velocity data were recorded, we captured the following series of images: 1) just before the splitting fork to document bead dispersion in droplets; 2) at the splitting fork to characterize the separation efficiency; 3) after the fork to measure the droplet volume ratio of the split droplets.

Bead dispersion in droplets. Using a macro developed under Fiji, we segmented each image of the series to locate droplets. We used a mask to crop droplets out of the image after subtracting a background image without droplet to remove illumination inhomogeneity. The processed images were aggregated into a stack from which we generated an average intensity projection that displays the general bead distribution of beads inside droplets, and a minimal intensity projection that highlights the location of single beads across the stack. Stacks were compiled from at least 45 images.

Separation efficiency. We characterized separation efficiency by counting the number of beads present in the “waste” droplets after splitting in a semi-automated way using Fiji. Distributions are compiled from at least 60 droplet images.

Droplet volume ratio. Droplet volume ratio was determined by segmenting droplet outlines from purposely over-exposed images. The area measurements of droplets were compiled into distributions that exhibited two separated sub-populations. The droplet volume ratio was calculated from the ratio of the distribution maxima of the 2 droplet populations. In almost all experiments droplets were squeezed into “pancakes” in which cases the ratio of projected areas is equal to the volume ratio. In one case, (1:1 splitting fork) droplets were not squeezed and we corrected the data by the following formula: $\text{droplet volume} \propto (\sqrt[2]{\text{projected area}})^3$, and then performed the ratio. We observed only a very small difference between droplet volume ratios in the presence or absence of the magnet. The difference is most likely due to a difference in the ability to segment droplets with a homogeneous distribution of beads (without magnet) or with a large bead aggregate present (in the presence of a magnet).

Fork study. To optimize the workflow and to reduce the number of splitting passes required to dilute the initial solution to the target concentration, we tested a series of different splitting forks. Fork designs studied here derive from the initial 1:1 fork that is made of two channels of equal width (25 μm), one in line with the re-injection channel and the second at a 45° angle away from the magnet. The two channels are joined back together after the splitting such that the pressure-drop is the same across both channels. In this case, flow splitting directly depends on the ratio of hydrodynamic resistance of the channels. The length of the channels are a couple of droplets long (500 μm) and experimental conditions are such that only one droplet is present in a channel at any given time. We tested three series of fork designs that differ by their hydrodynamic resistance ratios as a consequence of changing the width and length of the initial 1:1 fork (50 μm deep): 1) 1:3 split flow with 18 μm wide x 300 μm long: 32 μm wide x 340 μm long channels; 2) 1:5 split flow with 16 μm wide x 290 μm long: 34 μm wide x 300 μm long channels; 3) 1:7 split flow with 14 μm wide x 256 μm long: 36 μm wide x 300 μm long channels. In addition, in order to collect all the beads that tend to aggregate into the droplet lower front corner closer to the magnet we modified the previous designs by adding a first section similar to the 1:1 fork. This 25/25 μm section was either 25 μm or 50 μm long. To characterize the effect of the fork design on the way droplets are split we inferred the splitting profile for each of them from high-speed videos. Videos were taken at 600 frames per second with a Casio EX-F1 camera mounted onto one of the microscope ocular using an adapter (Zarf enterprises). Videos were converted into stacks of frames using ImageJ. The splitting profiles were reconstructed by measuring the projected areas of the droplet entering each channel over time (**Supp. Fig. 6**). We segmented each frame to extract the droplet shape and we measured the projected area of the droplet in each channel. Finally, we interpolated the projected area and the ratio of entrance rates over time for each channel. Interpolations were performed in Excel with either linear or polynomial functions. All interpolations had a R-squared value of at least 0.99.

High-speed analysis of the splitting generated by the addition of a 50 μm box to the 1:3 splitting fork.

Droplets were generated with hydrodynamic nozzle (50 μm wide and 25 μm deep) located at a distance of 2 droplet lengths prior to the splitting fork. Droplets are patterned by using a 1:3 dark:light co-flow to emphasize the details of the splitting. The dark solution is Bromophenol blue at 0.05% weight in PBS and the light solution is PBS. Images were captured with a high-speed video camera (X-PRI, AOS Technologies AG) at 500 frames per second. Consecutive frames are 2ms apart and the total sequence lasts 14ms, and the droplet velocity is 2.3 mm/s.

Magnets. Magnets used in this study are Neodymium magnets (K&J Magnetics), made of material grade N42 or N52.

Magnetic field simulation

We simulated the magnetic fields in the vicinity of our rare earth permanent magnet using a finite-element solver Maxwell 11.1 (Ansoft). During simulation runs we simultaneously calculated the B-field, and the gradient of the B-field using a mesh size of less than 100 μm in regions of interest. The simulations were carried out in a box of 1''x 1''x 1'' (Fig.1,2; Supp. Fig. 2).

1. D. C. Duffy, J. C. McDonald, O. J. A. Schueller and G. M. Whitesides, *Anal. Chem.*, 1998, 70, 4974-4984.
2. C. Holtze, A. C. Rowat, J. J. Agresti, J. B. Hutchison, F. E. Angile, C. H. Schmitz, S. Koster, H. Duan, K. J. Humphry, R. A. Scanga, J. S. Johnson, D. Pisignano and D. A. Weitz, *Lab Chip*, 2008, 8, 1632-1639.

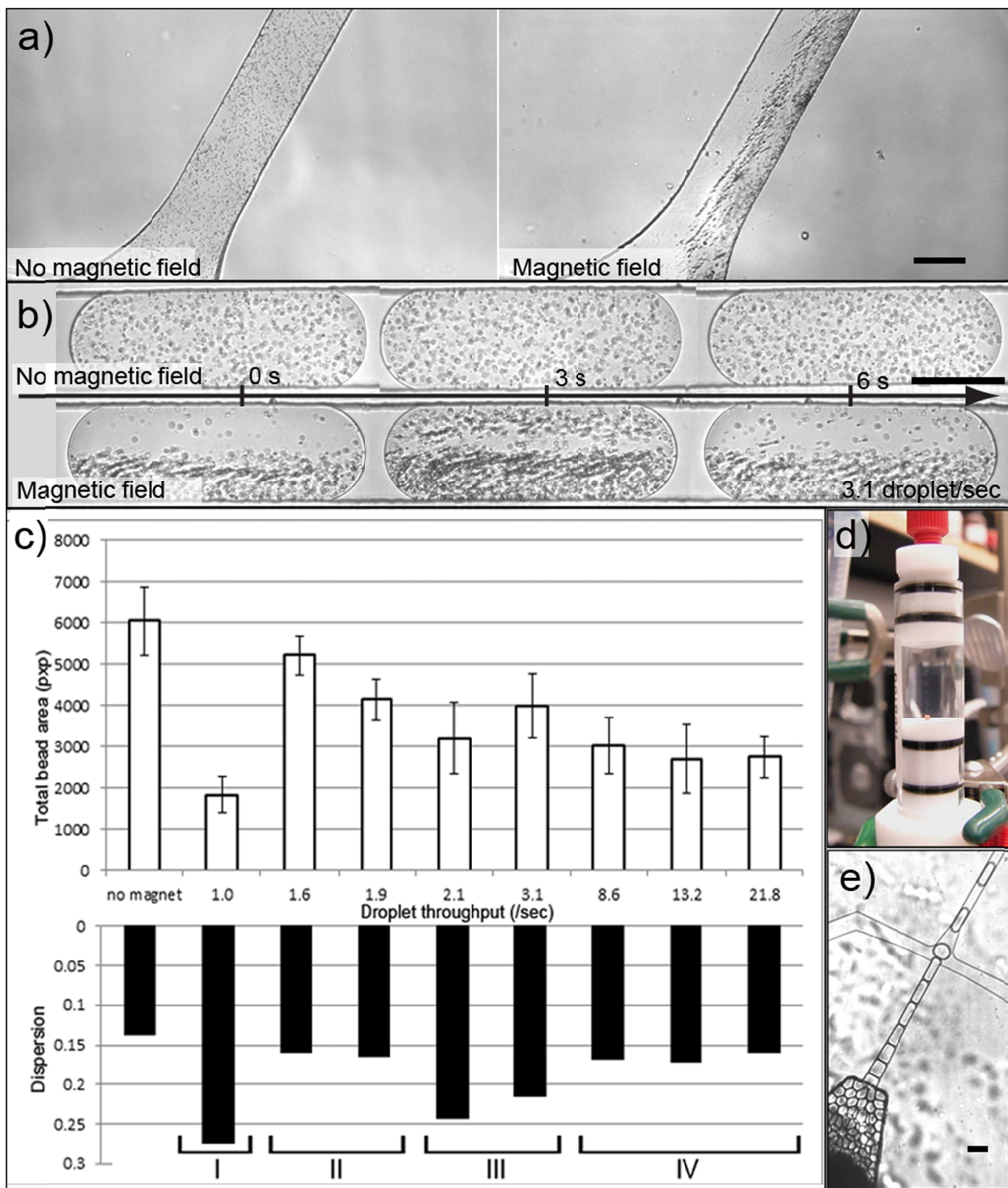
Supplemental movies.

Supp. Movie 1: Movie depicting the injection of magnetic beads into the microfluidic chip in absence of magnetic field (left panel), and in presence of a magnetic field. The movie is 2-fold accelerated.

Supp. Movie 2: Movie of a magnetic-laden droplet flowing at 3.9 mm/s in the absence of magnetic field. The movie is slowed down 70 fold and played at 7 frames per second.

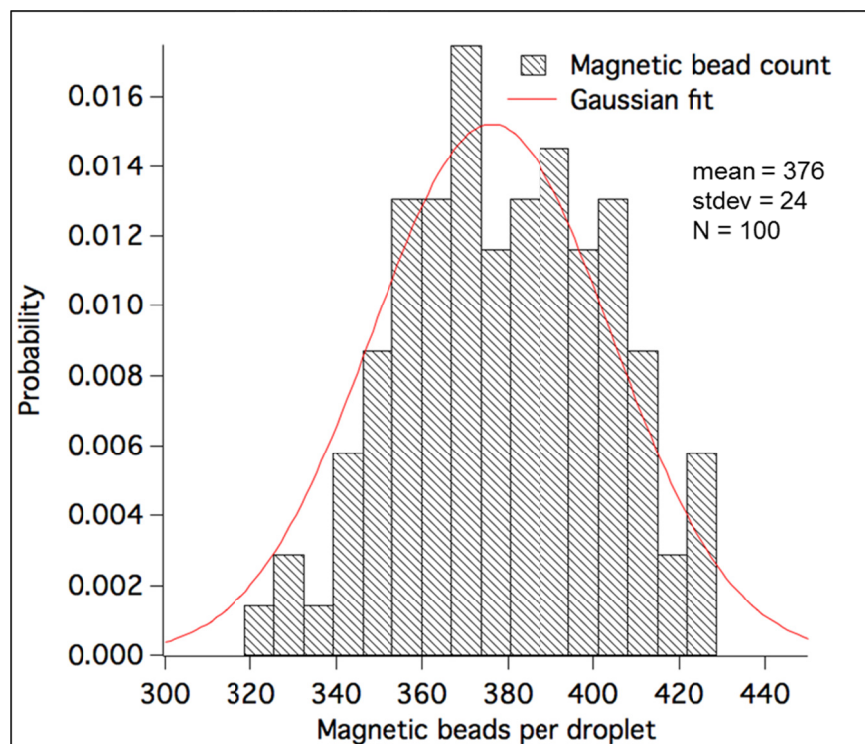
Supp. Movie 3: Movie of the splitting of a patterned droplet by the 1:3 splitting fork with a 50 μm box at 2.3 mm/s. The movie is slowed down 25 fold.

Supp. Movie 4: Movie of the splitting of a droplet by the 1:3 splitting fork with a 25 μm box at 1.46 mm/s, and a 50 μm box at 1.15 mm/s that respectively depict droplet retraction and the blockade of the small droplet daughter. The movie scenes have been accelerated 2 and 4 fold respectively.

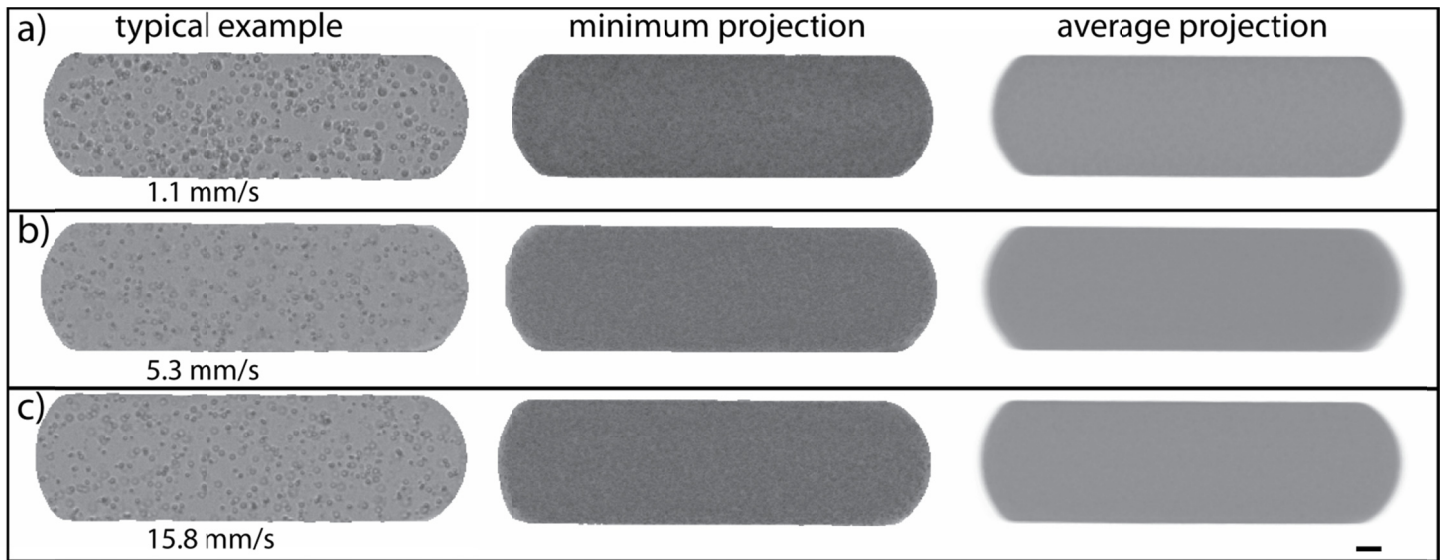


Supp. Fig. 1: Encapsulation of magnetic beads in presence of a magnetic field. a) View of the inlet before the droplet generating nozzle. The spatial distribution of magnetic beads in the absence of magnet is uniform and homogeneous (right); while magnetic beads form chains during injection in the presence of a magnet even

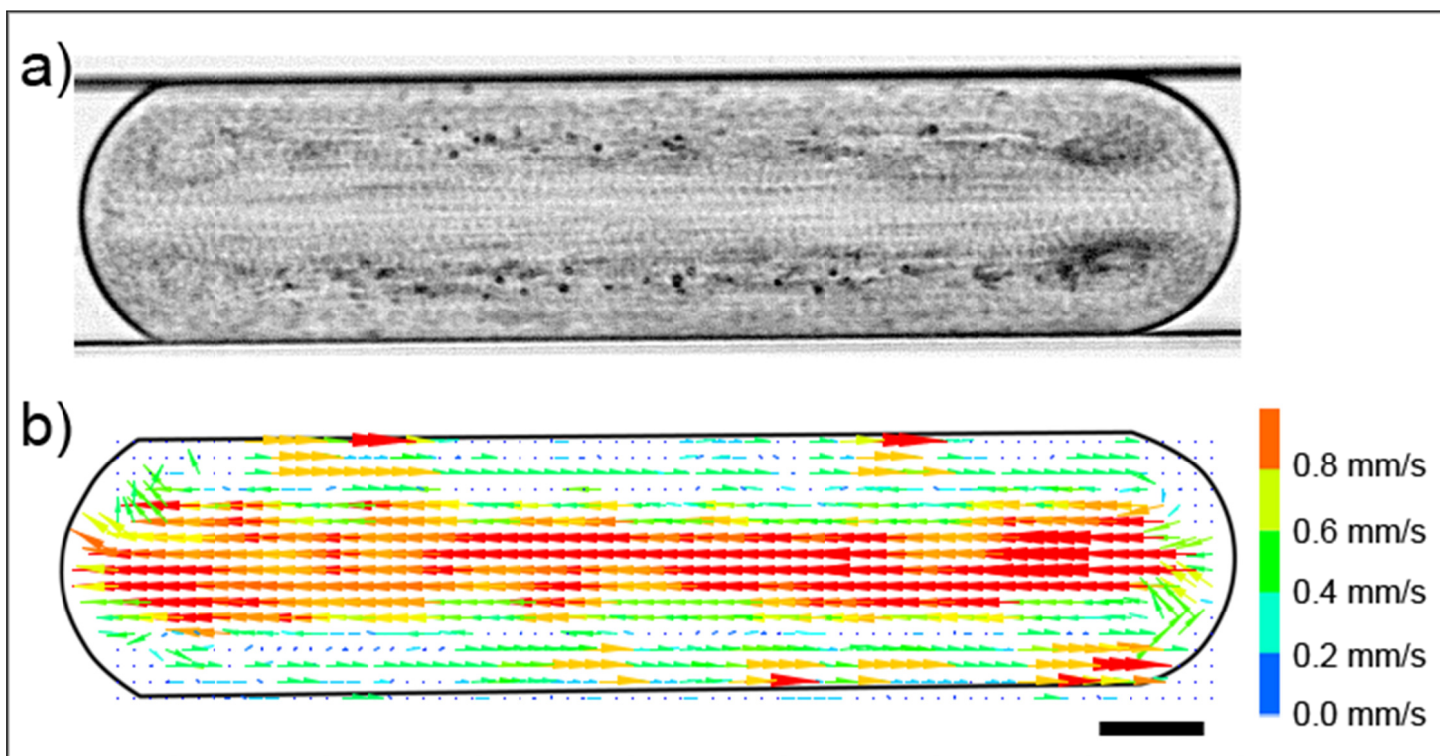
located at (distance) from the nozzle (left). b) The formation of chains result in an uneven flow of magnetic beads to the nozzle and cause a large variation of number of magnetic beads in droplets (lower panel); while the number of beads encapsulated remains in a tight range in the absence of a magnet (upper panel). c) The quantification of the number of magnetic beads encapsulated in the presence of a magnetic field shows that the average number and its dispersion depend on the droplet generation throughput. Only in the narrow range denoted II can one obtain an average number and dispersion of beads close to the condition without magnet. As a consequence, we generated and collected droplets without magnetic field (d), before re-injecting them in presence of a magnetic field (e) to maintain the number of magnetic beads constant while exploring the effect of droplet velocity on internal flow and their effect on the spreading of magnetic beads inside droplets. Scale bars in different panels represent 50 μ m.



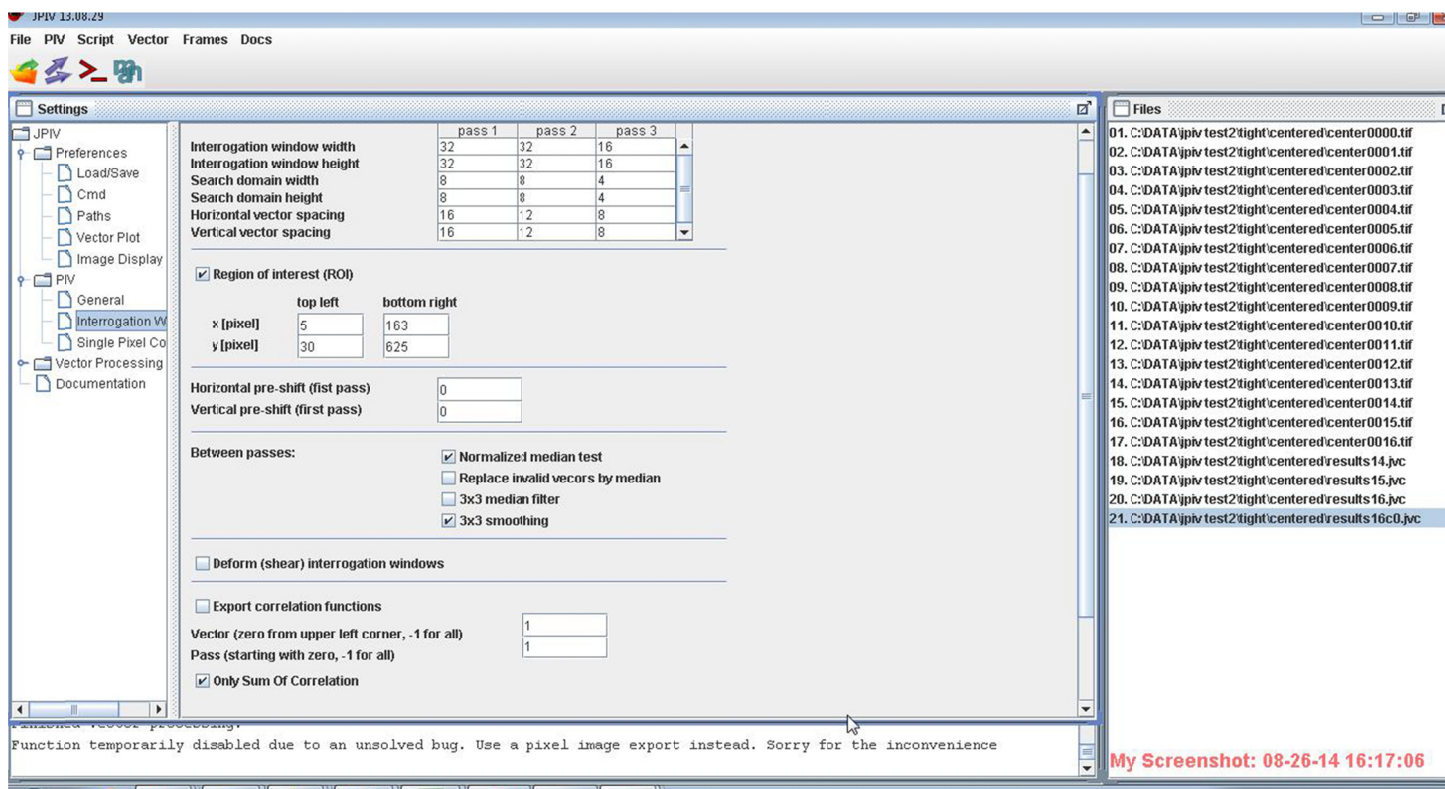
Supp. Fig. 2: Statistical distribution of the number of 1 μm magnetic beads per 185 pL droplet.



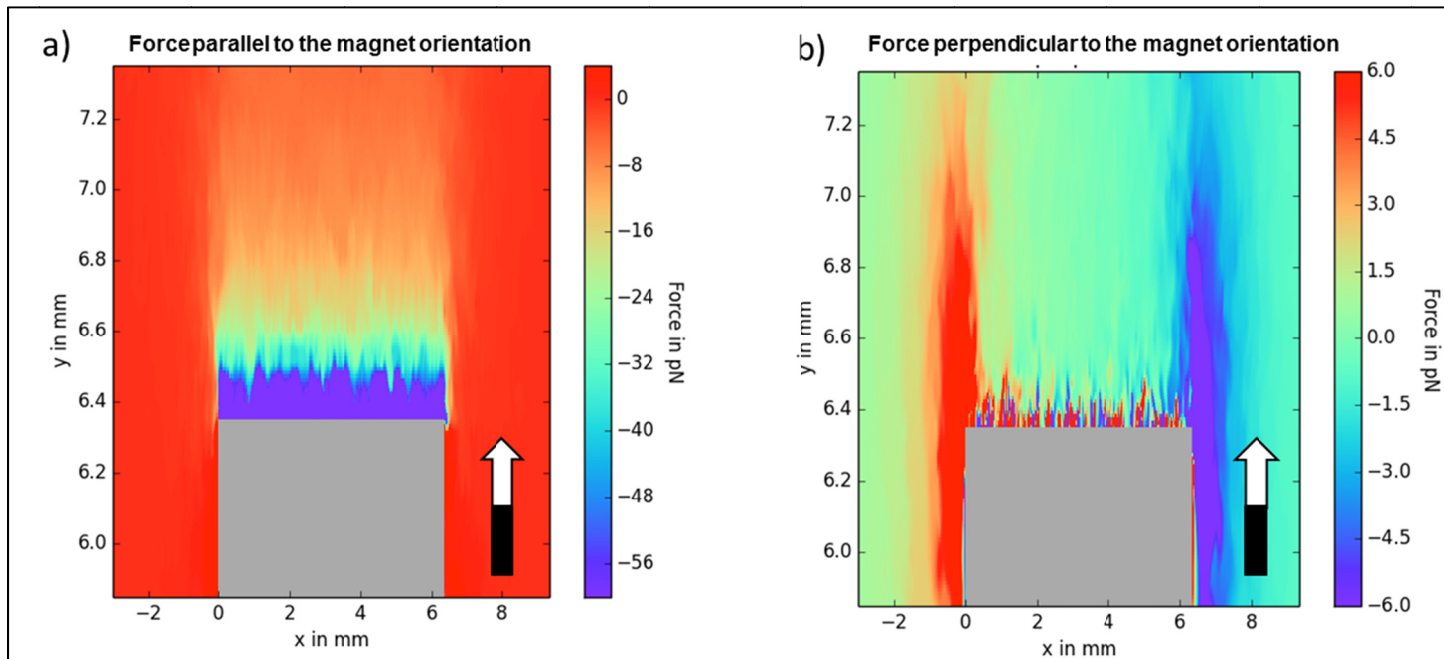
Supp. Fig. 3: Absence of marginalization of the magnetic beads in the absence of magnetic field. There is no inhomogeneous accumulation of magnetic beads inside droplets as a result of potential patterns of internal flows. Scale bar represents 10 μm .



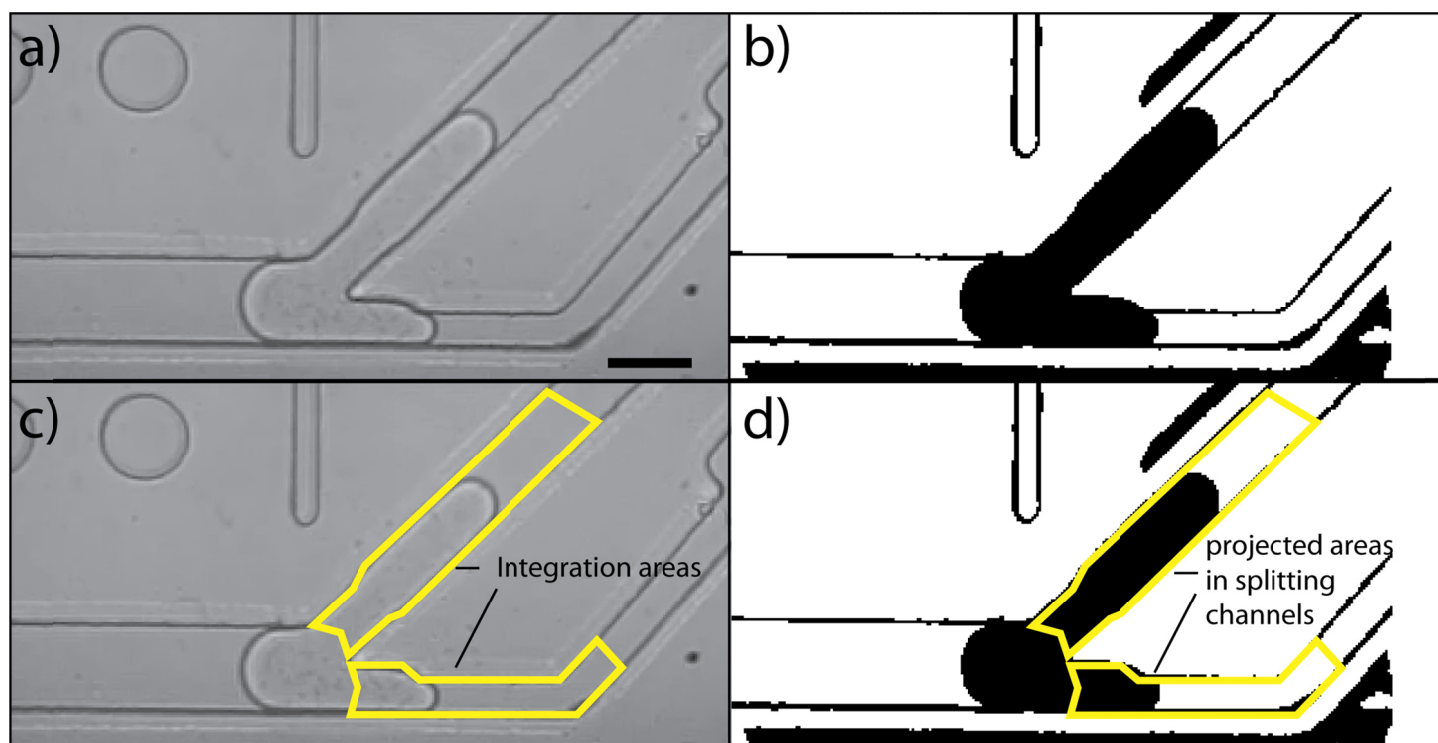
Supp. Fig. 4: Internal flow using magnetic beads as tracer particles in the absence of magnetic field. a) Average projection of the frames of Supp. Movie 2 reveals the absence of capturing vortex that could have trapped magnetic beads in absence of a magnetic field. b) A Particle-Image Velocimetry analysis further confirms the absence of trapping hydrodynamic patterns. Scale bar represents 20 μm .



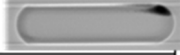
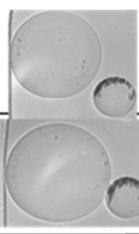


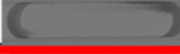



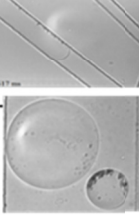





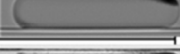
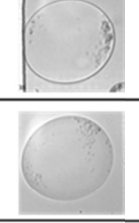





Supp. Fig. 5: Parameters used to perform PIV analysis on frames from Supp. Movie 2 using the JPIV package (www.jpiv.vennemann-online.de).



Supp. Fig. 6: Mapping of magnetic forces exerted by a permanent cubic (1/4") magnet N52 on a single magnetic bead. The arrows indicate the magnet orientation. a) magnitude of the magnetic force parallel to the magnet orientation; b) magnitude of the magnetic force perpendicular to the magnet orientation.



Supp. Fig. 7: Method to extract splitting profile from time-lapse series. a) images from a time-lapse series are processed to extract the droplet profile by thresholding (b). c) we define two areas that define the location of the channels. d) we measure the projected area of the droplet in each of the channel over the time-lapse series. We use this information to calculate the relative rate of entry of the droplet in the two branches and thus deduct the splitting profile.

| Split flow | Box size (mm) | Bead dispersion | | Separation efficiency |
|------------|---------------|--------------------|--|--|
| 1:3 | 0 | average projection |  |  |
| | | minimum projection |  | |
| | 25 | average projection |  | |
| | | minimum projection |  | |
| | 50 | average projection |  | |
| | | minimum projection |  | |
| 1:5 | 0 | average projection |  |  |
| | | minimum projection |  | |
| | 25 | average projection |  | |
| | | minimum projection |  | |
| | 50 | average projection |  | |
| | | minimum projection |  | |
| 1:7 | 0 | average projection |  |  |
| | | minimum projection |  | |
| | 25 | average projection |  | |
| | | minimum projection |  | |
| | 50 | average projection |  | |
| | | minimum projection |  | |

Supp. Fig. 8: Separation efficiency of a series of asymmetric splitting forks for a droplet velocity of 5 mm/s.